Deformation and fracture of micron-sized metal-coated polymer spheres: an in-situ study

Molly Bazilchuk[1,2], Takashi Sumigawa[3], Takayuki Kitamura[3], Zhiliang Zhang[1], Helge Kristiansen[1,2] and Jianying He[1*]

[1] *Department of Structural Engineering, Norwegian University of Science and Technology, Trondheim, 7491, Norway*

[2] *Conpart AS, Skjetten, 2013, Norway*

[3] *Department of Materials Science and Engineering, Kyoto University, Kyoto, Japan*

*Corresponding author: jianying.he@ntnu.no

Abstract

Micron-sized metal-coated polymer spheres are the dominant conductive component in anisotropic conductive adhesives for electronic interconnect. The interconnect is formed under compression, so an understanding of the deformation and fracture of the metal-coated polymer spheres is paramount in particle design for fine pitch applications. The fracture of metal-coated polymer spheres has previous been measured but not observed in-situ. Using a nanoindentation set-up mounted in a scanning electron microscope, 10 µm polymer spheres with Ni, Ni/Au, Au and Ag coatings were compressed and their behavior observed in-situ. The metal systems were observed to lead to fracture in two different modes, brittle and ductile. The fracture mode was not dependent on the type of metal, and not on the coating thickness. Additionally, the rate dependency of the mechanical behavior due to the viscoelastic polymer core was studied, and found to influence the deformation and stress-strain behavior around the fracture point.

Keywords: nanocomposites, nanoindentation, mechanical properties, fracture and fatigue

Introduction

Anisotropic conductive adhesive (ACA) is a composite material consisting of 5-10 vol% of a conductive filler mixed in an adhesive matrix, typically epoxy [1]. ACA is commonly used in electronic assembly applications that require fine pitch coupled with low temperature processing, or where materials not wet by traditional solder are used, such as display manufacturing [2]. During ACA bonding, the adhesive is compressed between a chip and a substrate, and filler particles are trapped between corresponding bumps. This enables anisotropic conductivity, since current is carried across bumps but not in plane, as illustrated in Fig. 1.
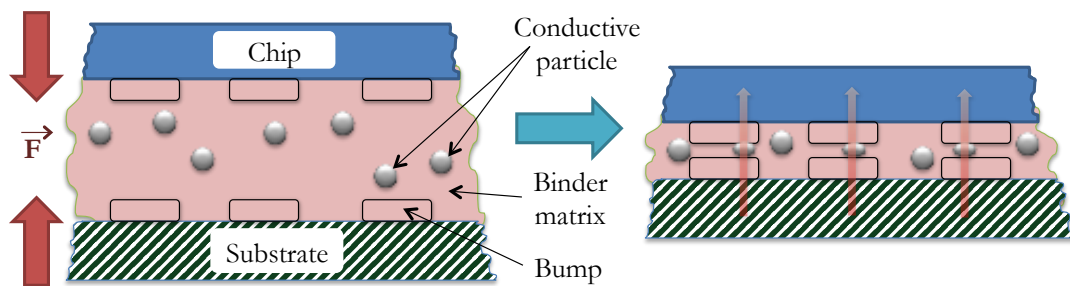

Figure 1: A schematic of ACA bonding [3], during which the chip and substrate are brought together under applied force and heat. Conductive particles are trapped between corresponding bumps, creating conductive paths across the bumps but not between them.

Micron-sized metal-coated polymer spheres (MPS), 3-10 µm in diameter with nanoscale metal coatings, are a common conductive filler component in ACA [2]. Conventional ACA employs MPS coated with a nickel-gold bilayer [4]. MPS deform elastically up to a large deformation compared to solid metal filler, providing more mechanical compliance and thus improved reliability [5].

To form a reliable, highly conductive electrical interconnect, the MPS must have a sufficiently large contact surface to the pad and bump on either side [6]. For this reason, the electrical resistance through the interconnect is strongly linked to the deformation state of the particles. This is further demonstrated in experimental studies that show a strong dependency between the ACA bonding pressure and the electrical resistance in bonded components [4, 7, 8]. Fracture in the core or coating of the MPS may lead to increased electrical resistance during reliability testing [4, 6]. Analysis of the large deformation characteristics as well as the onset of fracture are therefore key in understanding and optimizing the performance of MPS in ACA.

He et al. developed a flat punch nanoindentation technique to characterize the mechanical behavior of individual MPS in air [10]. Rapid displacement bursts in the force-deformation curve, known as pop-ins, have been linked to fracture events in the MPS [11]. The fracture of 3.8 µm nickel-gold coated MPS has been studied at different loading rates, and the loading rate was found to influence the cracking direction of the metal coating [12]. The flat punch nanoindentation technique has been further extended to include simultaneous electrical characterization [13].

As the demands to pitch and performance in ACA increase, the industry looks to novel MPS materials, and it is important to understand the influence of the metal coating on particle deformation. Fracture of the metal coating perpendicular to the direction of compression could sever the contact, leading to failure of the interconnect. Constable et al. found that MPS cracked parallel to the direction of compression [14] , while findings reported by He et al. indicated that the crack direction depending on the loading rate due to the viscoelastic nature of the polymer core [12]. In both studies, the cracks were observed ex-situ. An in-situ study of MPS compression will allow direct correlation of events in the mechanical data to MPS morphology, as well as revealing changes not visible from the mechanical data alone, such as the onset of delamination and smaller fracture events.

Several studies have attempted to model fracture in MPS. Applying the cohesive zone model, a finite element study of a nickel-coated MPS predicted that the metal coating should form two symmetric cracks parallel to the direction of compression [15]. It should be noted that cohesive elements in this model were only placed along a ring running pole-to-pole in the MPS, so the areas where cracks could form were in fact predetermined. Molecular dynamics (MD) simulations on polyethylene particles with nickel coatings predicted failure of the metal coating starting at high nominal strain of 0.4, due to perfect adhesion and coating structure [16]. Neither the finite element nor the MD study could predict delamination of the metal from the core. X-ray imaging performed on silver-coated MPS with moderately cross-linked acrylate methacrylate copolymer cores indicated that global delamination at the metal-polymer interface does in fact occur and may begin before cracking of the metal coating [17].

This work is an experimental study of the deformation and fracture of MPS for ACA applications. Using in-situ SEM imaging of flat punch compression tests, the deformation and fracture of MPS with four different coatings (nickel, nickel-gold, gold and silver) are

analyzed. Loading rate dependency, stemming from the viscoelastic polymer core, has also been studied. A preliminary study of a similar nature was performed by Tao [18], however only one type of particle was considered.

Experimental

The Hysitron Picoindenter 85L (Minneapolis, USA) is a nanomechanical test instrument that is designed to be mounted in a scanning electron microscope (SEM). The module allows for precise force-displacement measurements to be performed while continuously imaging with an electron beam. The Picoindenter was mounted in a Hitachi SU8230 SEM (Tokyo, Japan). A custom diamond flat punch tip, 20 µm in diameter, was fabricated from a Hysitron conical punch using a focused ion beam.

The MPS used in this study were provided by Conpart AS (Skjetten, Norway). The monodisperse polymer cores are fabricated using the Ugelstad method [19]. All the MPS had cores from the same batch of styrene cross-linked with 20% DVB polymer core. The cores were 9.7 µm in diameter with coefficient of variance $< 2\%$, measured by Coulter counter. The cores were coated with metal using electroless plating. The metal coatings investigated were silver, nickel, gold and nickel-gold bilayer, with thicknesses ranging from 30-150 nm. Since all particles have the same core, we will refer to different batches using their metal coating type and thickness, e.g. Ni90. All metal thicknesses are nominal, calculated from the total amount of metal ions in the solution. The nickel used in both nickel and nickel-gold coatings was deposited using phosphorus as reducing agent. The MPS were dispersed in ethanol and the suspension dried onto a clean polished silicon substrate, which was subsequently glued to the Picoindenter stub using silver paste.

To maximize imaging clarity, the Picoindenter was tilted 2° towards the electron beam during compression tests. Before testing, the tip was manually stepped towards the surface until the force display as well as visual SEM confirmation indicated tip-particle contact. The tip was then stepped back 100-500 nm from the surface of the particle from whence the compression test was conducted. The measurements were performed in displacement control. The standard loading and unloading rate was 100 nm/s, while rates of 10 and 1000 nm/s were also used to investigate viscoelastic effects stemming from the polymer core. The maximum

displacement of the particles was limited to a maximum of 5 µm by constraints in the transducer, corresponding to approximately 50% nominal strain of the particles. Each compression test was capture as a film at 20 frames per second.

SEM imaging was conducted at a relatively low acceleration voltage of 3kV to minimize charging and Joule heating of the sample. Charging artefacts were only observed in the cases where the metal coating fractured and the polymer core was exposed. This indicates that the contact between the metal coating and the silicon substrate was sufficient to prevent significant charging effects.

After compression testing, each sample was imaged from above (relative to the direction of compression) in a Hitachi S 5500 SEM. A coordinate system was used to identify the MPS that had been compressed and image them from above. Since the images obtained in the Picoindenter only show half of the particle, imaging the sample from above enables the observation of cracks obscured during compression. The samples were typically imaged 12-24 hours after the compression testing, during which some degree of recovery occurred. They were stored in ambient conditions between compression and imaging.

Results and Discussion

Two modes of MPS fracture were observed, which we shall refer to as brittle and ductile. The brittle mode was characterized by major cracks and global delamination of the metal coating from the polymer core (see Fig. 1), while the ductile mode was characterized by microcracks with no global delamination of the metal coating (see Fig. 5). The Ni and Ni-Au MPS fractured consistently in the brittle mode, while the Ag and Au MPS fractured in the ductile mode.

The nominal stress σ and strain ε were calculated based on the measured force F and the applied deformation δ using the following relationships:

$$\sigma = \frac{F}{\pi R^2} \tag{1}$$

$$\varepsilon = \frac{\delta}{2R} \tag{2}$$

where R is the radius of the undeformed MPS, found by summing half of the diameter of the polymer core with the nominal metal thickness.

Fig. 2 shows a typical example of an MPS before (a) and after (b, d) compression and fracture in the brittle mode, with the corresponding stress-strain curve (c). The particle in Fig. 2 is Ni90 but the deformation and fracture behavior is representative for all those with Ni and NiAu coatings. Cracks are unstable and propagate rapidly after initiation, faster than the frame rate of imaging. Widespread delamination at the metal-polymer interface is clearly visible as soon as the crack propagates. Nanocrystalline phosphorus nickel materials are known to exhibit brittle fracture [20]. Given that the brittle mode of fracture was unique for coatings containing nickel, we conclude that the brittle nature of the phosphorus nickel layer dominated the fracture pattern in both Ni and Ni/Au MPS.

The stress-strain curve in Fig. 2c exhibits stress drops (points c1 and c2) in the otherwise monotonously increasing loading portion. Examination of the in-situ video provided a positive correlation between these stress drops and the appearance of cracks. In the cases where cracks were formed on the obscured half of the particle, the flat punch appeared to pause as the feedback loop compensated for the sudden change in particle stiffness before displacement continued. The obscured crack could be identified during the post-compression imaging. During crack propagation, the metal coating loses most of its load bearing capacity, and the force is suddenly transferred to the softer polymer core, causing the change in gradient observed in the stress-strain curves.

In previous studies, where measurements have been performed in load control, displacement bursts (pop-ins) have been correlated to coating fracture [11]. In load control, the transfer of force from the metal coating to the polymer core necessitates rapid displacement to continue increasing the force. In displacement control as used in this work, the sudden loss of load bearing capacity requires the feedback loop to rapidly decrease the amount of force to try to keep the deformation rate constant. The stress drops are thus analogous to the previously described pop-ins. The electronic feedback loop of the transducer was not able to keep up with the sudden drop in force, resulting in a decrease in strain along with the stress drop as apparent near point c1 in Fig. 2c.
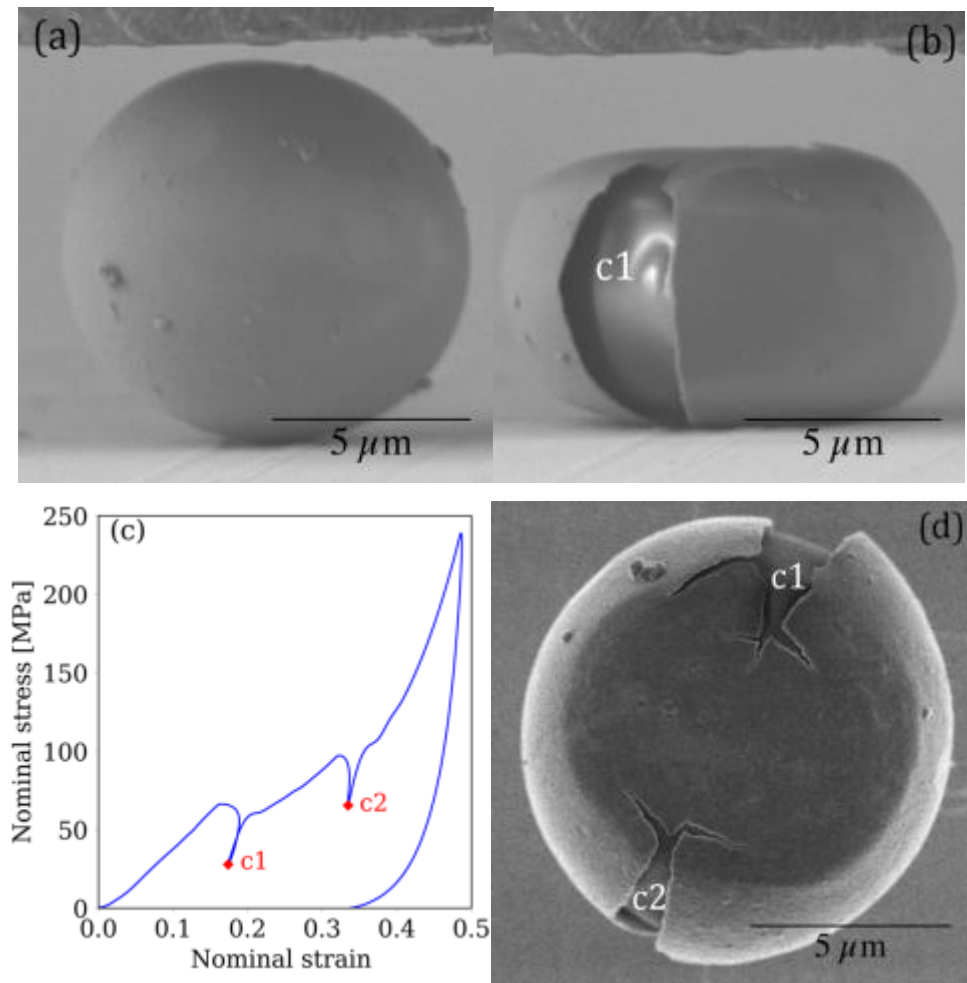
Figure 2: Deformation and fracture of a Ni90 particle, (a) before compression; (b) directly after compression;(c) the corresponding stress-strain curve; and (d) the same particle imaged from above. Corresponding cracks are labelled in each of the images.

A total of two (Fig. 2) to three (Fig. 3) cracks formed in the coating of each brittle MPS. The two primary cracks were located almost directly opposite each other. In MPS where a third crack appears, it was roughly equidistant from the two initial cracks. Global delamination at the metal-polymer interface was most prominent in the two initial cracks. Since the third crack only appeared near the highest applied deformation, it is possible that delamination would continue around this crack at even higher loads. The tertiary crack did not result in a stress drop like the primary cracks, probably since almost all the load has already been transferred to the polymer core after the second crack.
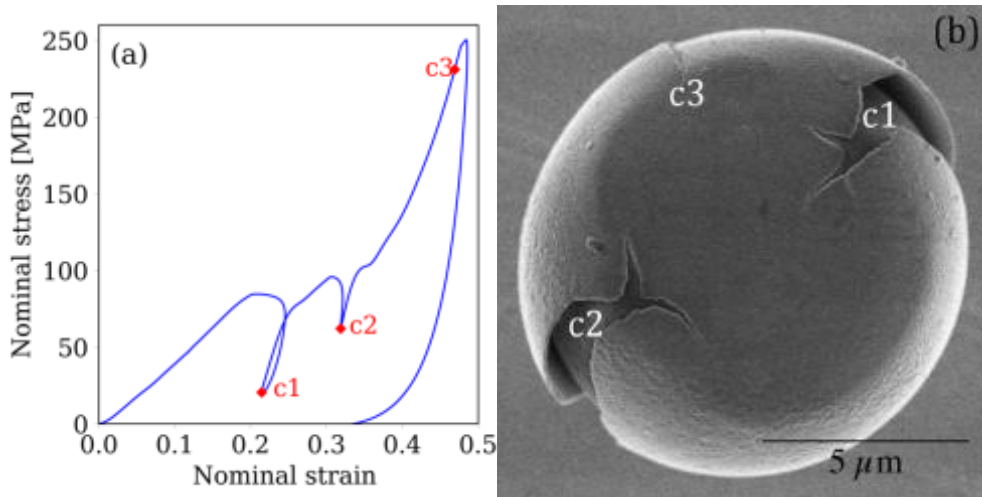
Figure 3: A stress-strain curve (a) and post-compression image (b) of a Ni90 particle which has cracked thrice rather than twice. The tertiary crack (labelled c3) does not results in a stress drop as seen in c1 and c2.

It should be noted that the initial fracture sites may have been influenced by misalignment between the tip and the substrate. The misalignment was found to be roughly 3-4° in the setup, and the Picoindenter does not have a method to adjust the coplanarity between the substrate and the tip. This asymmetric loading would concentrate stress on half of the particle, making it more likely to fracture.

The strain at first fracture is defined as the strain at the final data point before the stress begins to drop rapidly. Analysis of the strain at first fracture for the brittle particles examined in this study are summarized in Tab. 1. The first fracture occurred between 12 and 23% strain, with an overall average of 16.7%. This is within the range of the experimental findings of He et al. [12]. However, the variation in average strain at first fracture between different particle thicknesses and metallization was statistically significant. The addition of the gold layer was not observed to affect the fracture process significantly, indicating that the fracture is dominated by the nickel layer. No correlation between the strain at first fracture and the total thickness of the metal coatings was observed. However, the metal thickness in all cases was less than 3% of the core diameter, so the variations in coating thickness may be too small to influence the fracture behavior.

Table 1: The average strain at first fracture for MPS with nickel in the coating.

MPS	Average strain at first fracture
Ni60	16.0±1.1%
Ni90	18.2±2.1%
Ni120	15.7±1.7%
Ni90Au5	18.7±2.4%
Ni90Au15	16.2±1.2%
Ni90Au20	15.8±1.9%
Ni90Au30	16.7±1.8%

In many instances, small holes or defects were visible in the metal coatings. In these cases, the crack always passed through the defect. A commonly observed defect was a welding hole, which results from two MPS forming a metallurgical bond during the plating process and then being mechanically separated. Fig. 4a shows an example of a Ni90 particle with a welding hole, and in the post-compression image Fig. 4b we can clearly see that the fracture line passed directly through the hole. Structural defects such as holes are expected to act as stress concentration sites, and therefore are the weakest area in a coating. From the observation in the case of welding holes, we infer that defects in the coating, rather than bulk material parameters, drive the fracture process, which contributes to the seemingly random spread of strains at first fracture.
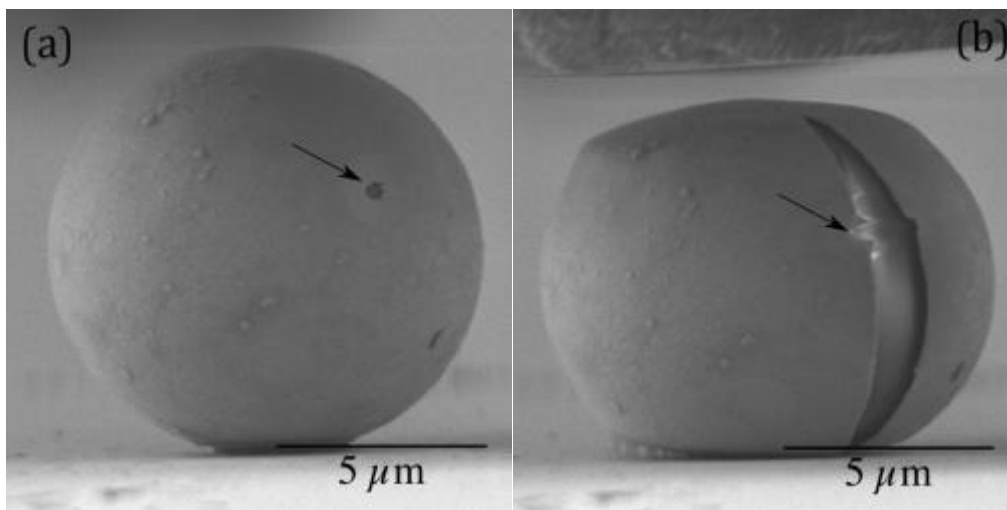
An example of deformation in ductile mode of a Au40 can be seen in Fig. 5. In the ductile mode, the metal coating exhibited microcracks at high (>45%) strains, with no global delamination. The coating shown in Fig. 5 had several preexisting holes, and microcracking occurs through these regions as in the brittle case. Due to recovery of the polymer core during unloading, the microcracks closed and the polymer core remained covered. Both the pure gold and silver coatings exhibited ductile behavior at all loading rates examined. The microcracking phenomenon was more pronounced in thinner coatings.
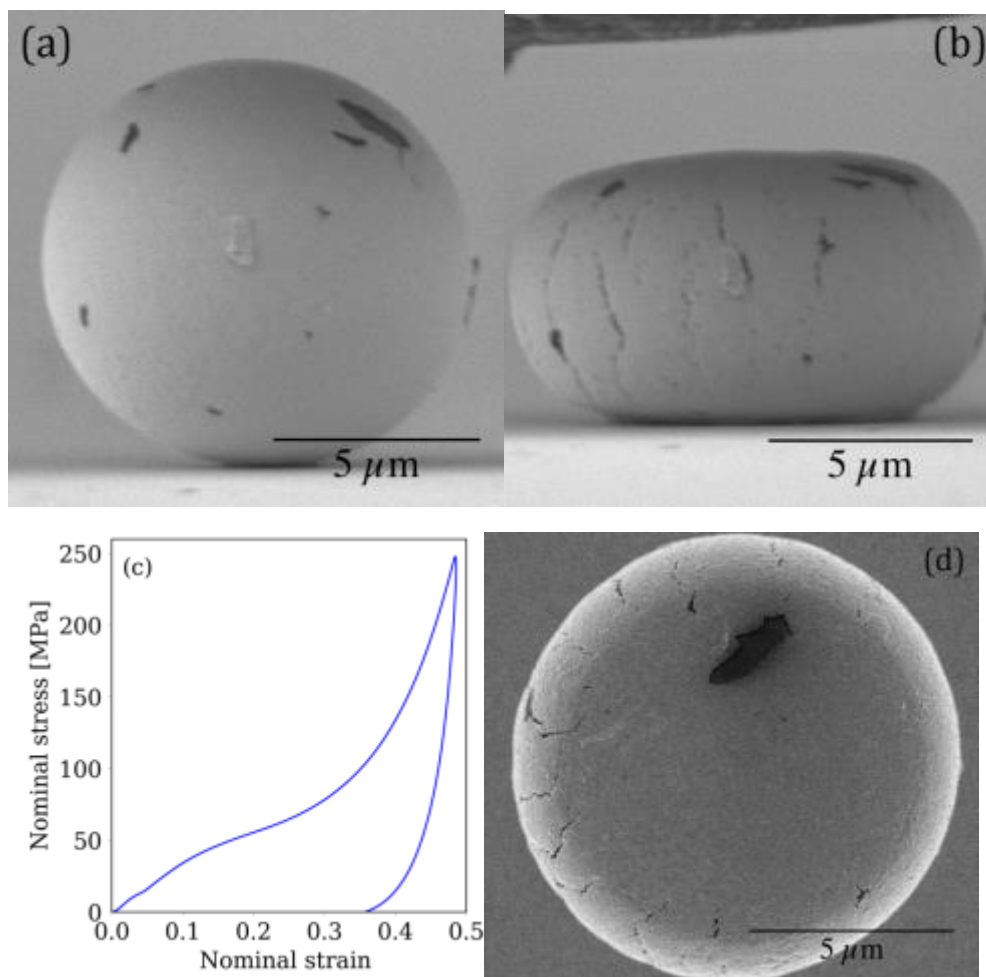
The stress-strain curve in Fig. 5c shows monotonically increasing stress during loading, without the stress drops characteristic of the brittle mode. The cracks visible in Figs.

5b and 5d did not correlate to any distinctive behavior on the stress-strain curve. The unloading behavior was similar in the brittle and ductile curves.

Fig. 6 compares the stress-strain curves at different loading rates for a ductile MPS (Au40) and a brittle MPS (Ni90/Au30). Three different loading rates (10, 100, 1000 nm/s) were applied to observe the effect of the viscoelastic properties of the polymer core on deformation and fracture. At low strains (<0.05), the stress-strain curves were not rate dependent. During the initial phase of loading, the contact area between the probe and the MPS is very small. This causes locally high stress in the contact area, which will lead to plastic deformation of the metal coating. It is possible that the deformation of the metal coating dominates over the viscoelasticity of the core at low strains. This effect would be further magnified for rough particle surfaces, as the probe could only be touching the particle in a few points initially.

Above strains of 0.05, both brittle and ductile MPS display a clear deformation rate dependency typical of viscoelastic polymers. For the ductile system (Fig 6a), this rate dependency continues for the duration of deformation, indicating that the polymer core dominates the deformation.

In Fig. 6b, we observe that the characteristics around the stress drop in the brittle system appear to depend on the loading rate. At 1000 nm/s, a large shoulder appears before the stress drop, while at 10 nm/s the gradient of the curve changes without a shoulder. Upon further examination, we discovered that the deformation rate increased significantly around the stress drop. Since the deformation rate should have been constant, this is an artefact of the transducer feedback. The deviation from the set deformation rate was larger for higher deformation rates, lead to the pronounced shoulder artefact observed in Fig. 6b.
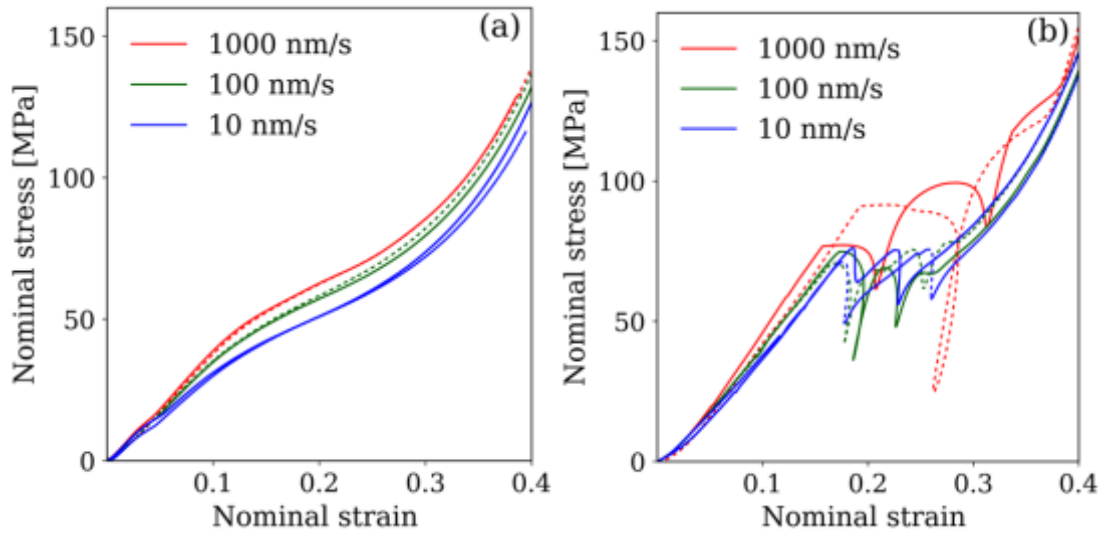
Figure 6: Stress-strain curves of two particles (solid and dashed lines) each of the deformation rates: 1000 nm/s, 100 nm/s and 10 nm/s for (a) Au40 (a ductile MPS) and (b) Ni90Au30 (a brittle MPS).

After first stress drop in the brittle system, the deformation rate dependency disappears. After the fracture, the transducer continues applying deformation, but continues from the bottom of the stress drop. The continuation of the stress-strain curve after brittle fracture depends more on the reaction speed of the transducer, than on the viscoelastic properties of the polymer.

In contrast to the findings of He et al. [12], all observed crack formation was parallel to the direction of loading, regardless of the loading rate. It should be noted that the polymer core of the MPS in He et al.'s work was acrylic rather than styrene based, and 3.8 µm rather than 10 µm in diameter. The adhesion between the metal coating and the polymer is key in fracture, and may vary depending on the polymer core. Furthermore, He's observations were not in-situ, and so correlations between loading curves and crack formation were inferred rather than observational.

The crack formation parallel to the direction of loading is significant because these cracks will not disturb the electrical conduction in an ACA application. When designing MPS for ACA applications, the use of the brittle system could be advantageous since the onset of fracture is a clear indicator that a strain in the range of 12-23% has been achieved. The cracks can then be used as a sort of strain gauge.

Conclusion

Metal-coated polymer spheres (MPS) with nickel-gold, nickel, silver and gold coatings have been compressed using a flat punch nanoindenter technique with in-situ SEM imaging. The images have been used to correlate stress drops in stress-strain curves with fracture events in the MPS' coating. The MPS coated with nickel or nickel-gold were found to fracture in a brittle manner, with global delamination at the polymer-metal interface. This is consistent with the brittle nature of the phosphorus nickel typical of electroless plating. The gold and silver coatings deformed in a ductile manner, and only presented microcracks at large strains. All fractures lines were observed parallel to the direction of compression, which would not hinder electrical conductivity. Since the MPS have a viscoelastic core, the deformation rate influences the gradient of the stress-strain curve at strains above 0.05. However, the deformation rate was not found to influence the placement or strain at the onset of fracture. This, in correlation with the apparent independence of the fracture strain on the coating thickness, leads us to conclude that the fracture strain is determined by defects in the coating rather than global factors. We have also observed cracks propagating from or through visible holes in the coating, further corroborating this hypothesis.

Acknowledgement

References

[1]   S.-C. Kim and Y.-H. Kim, "Review paper: Flip chip bonding with anisotropic conductive film (ACF) and nonconductive adhesive (NCA)," *Curr. Appl. Phys.*, vol. 13, pp. S14–S25, Jul. 2013.

[2]   Y. C. Lin and J. Zhong, "A review of the influencing factors on anisotropic conductive adhesives joining technology in electrical applications," *J. Mater. Sci.*, vol. 43, no. 9, pp. 3072–3093, 2008.

[3]   O. M. Evenstad, "Two Novel Methods in the Electrical Characterisation of Single

Metal-Coated Polymer Spheres," Norwegian University of Science and Technology, 2017.

[4]   C. K. Chung, G. D. Sim, S. B. Lee, and K. W. Paik, "Effects of conductive particles on the electrical stability and reliability of anisotropic conductive film chip-on-board interconnections," *IEEE Trans. Components, Packag. Manuf. Technol.*, vol. 2, no. 3, pp. 359–366, 2012.

[5]   M. J. Yim and K. W. Paik, "The contact resistance and reliability of anisotropically conductive film (ACF)," *IEEE Trans. Adv. Packag.*, vol. 22, no. 2, pp. 166–173, 1999.

[6]   Z. L. Zhang, H. Kristiansen, and J. Liu, "A method for determining elastic properties of micron-sized polymer particles by using flat punch test," *Comput. Mater. Sci.*, vol. 39, no. 2, pp. 305–314, Apr. 2007.

[7]   F. G. Shi, M. Abdullaht, S. Chungpaiboonpatanal, K. Okuyama, C. Davidson, and J. M. Adams, "Electrically Anisotropic Conductive Adhesives : A New Model for Conduction Mechanism," in *1999 International Symposium on Advanced Packaging Materials*, 1999, pp. 163–168.

[8]   W.-S. Kwon, S.-J. Ham, and K.-W. Paik, "Deformation mechanism and its effect on electrical conductivity of ACF flip chip package under thermal cycling condition: An experimental study," *Microelectron. Reliab.*, vol. 46, no. 2–4, pp. 589–599, Feb. 2006.

[9]   W. Kwon and K. Paik, "Experimental Analysis of Mechanical and Electrical Characteristics of Metal-Coated Conductive Spheres for Anisotropic Conductive," *IEEE Trans. Components Packag. Technol.*, vol. 29, no. 3, pp. 528–534, 2006.

[10]   J. Y. He, Z. L. Zhang, and H. Kristiansen, "Nanomechanical Characterization of Single Micron-Size Polymer Particles," *J. Appl. Polym. Sci.*, vol. 113, no. 3, pp. 1398–1405, 2009.

[11]   J. Y. He, T. Helland, Z. L. Zhang, and H. Kristiansen, "Fracture of micrometre-sized Ni/Au coated polymer particles," *J. Phys. D. Appl. Phys.*, vol. 42, no. 8, p. 85405, Apr. 2009.

[12]   J. Y. He, S. Nagao, H. Kristiansen, and Z. L. Zhang, "Loading rate effects on the fracture of Ni/Au nano-coated acrylic particles," *Express Polym. Lett.*, vol. 6, no. 3, pp. 198–203, Jan. 2012.

[13]   M. Bazilchuk, S. R. Pettersen, H. Kristiansen, Z. Zhang, and J. He, "Electromechanical characterization of individual micron-sized metal coated polymer particles," *J. Appl. Phys.*, vol. 119, no. 24, 2016.

[14]   J. H. Constable, "Analysis of the Constriction Resistance in an ACF Bond," *IEEE*

Trans. Components Packag. Technol., vol. 29, no. 3, pp. 494–501, 2006.

[15]   B. Xie, X. Q. Shi, H. Ding, and S. Member, "Investigation of Mechanical and Electrical Characteristics for Cracked Conductive Particle in Anisotropic Conductive Adhesive (ACA) Assembly," vol. 31, no. 2, pp. 361–369, 2008.

[16]   J. Wu, S. Nagao, Z. Zhang, and J. He, "Deformation and Fracture of Nano-sized Metal-coated Polymer Particles : A Molecular Dynamics Study."

[17]   J. Bø Fløystad, E. T. B. Skjønsfjell, M. Guizar-Sicairos, K. Høydalsvik, J. He, J. W. Andreasen, Z. Zhang, and D. W. Breiby, "Quantitative 3D X-ray Imaging of Densification, Delamination and Fracture in a Micro-Composite under Compression," *Adv. Eng. Mater.*, p. n/a-n/a, 2015.

[18]   J. Tao, "Novel Fine Pitch Interconnection Methods Using Metallised Polymer Spheres," 2016.

[19]   J. Ugelstad, a. Berge, T. Ellingsen, R. Schmid, T.-N. Nilsen, P. C. Mørk, P. Stenstad, E. Hornes, and Ø. Olsvik, "Preparation and application of new monosized polymer particles," *Prog. Polym. Sci.*, vol. 17, no. 1, pp. 87–161, 1992.

[20]   S. Kobayashi and Y. Kashikura, "Grain growth and mechanical properties of electrodeposited nanocrystalline nickel-4.4mass% phosphorus alloy," *Mater. Sci. Eng. A*, vol. 358, no. 1–2, pp. 76–83, 2003.

[21]   J. Paul, S. Romeis, J. Tomas, and W. Peukert, "A review of models for single particle compression and their application to silica microspheres," *Adv. Powder Technol.*, vol. 25, no. 1, pp. 136–153, Jan. 2014.